ORGANIC PROCESS RESEARCH & DEVELOPMENT
OPR&D
Article
pubs.acs.org/OPRD

Continuous Photo-Oxidation in a Vortex Reactor: Efficient Operations Using Air Drawn from the Laboratory

Darren S. Lee,[†] Zacharias Amara,[†] Charlotte A. Clark,[†] Zeyuan Xu,[‡] Bruce Kakimpa,[‡] Herve P. Morvan,[‡] Stephen J. Pickering,[‡] Martyn Poliakoff,*[,†] and Michael W. George*[,†,§]

[†]School of Chemistry, [‡]Department of Mechanical, Materials and Manufacturing Engineering, University of Nottingham, University Park, Nottingham, NG7 2RD, U.K.

[§]Department of Chemical and Environmental Engineering, University of Nottingham Ningbo China, 199 Taikang East Road, Ningbo 315100, China

Supporting Information

ABSTRACT: We report the construction and use of a vortex reactor which uses a rapidly rotating cylinder to generate Taylor vortices for continuous flow thermal and photochemical reactions. The reactor is designed to operate under conditions required for vortex generation. The flow pattern of the vortices has been represented using computational fluid dynamics, and the presence of the vortices can be easily visualized by observing streams of bubbles within the reactor. This approach presents certain advantages for reactions with added gases. For reactions with oxygen, the reactor offers an alternative to traditional setups as it efficiently draws in air from the lab without the need specifically to pressurize with oxygen. The rapid mixing generated by the vortices enables rapid mass transfer between the gas and the liquid phases allowing for a high efficiency dissolution of gases. The reactor has been applied to several photochemical reactions involving singlet oxygen ($^1O_2$) including the photo-oxidations of α-terpinene and furfuryl alcohol and the photodeborylation of phenyl boronic acid. The rotation speed of the cylinder proved to be key for reaction efficiency, and in the operation we found that the uptake of air was highest at 4000 rpm. The reactor has also been successfully applied to the synthesis of artemisinin, a potent antimalarial compound; and this three-step synthesis involving a Schenk-ene reaction with $^1O_2$, Hock cleavage with H^+, and an oxidative cyclization cascade with triplet oxygen ($^3O_2$), from dihydroartemisinic acid was carried out as a single process in the vortex reactor.

INTRODUCTION

Continuous flow chemistry is an increasingly popular alternative to traditional synthetic batch operations in both academic[1,2] and industrial settings.[3,4] As new developments are made in synthetic methodology, fine chemical, and active pharmaceutical ingredient (API) synthesis, there is parallel interest in translating these methodologies to continuous processes.[5] Continuous flow chemistry can provide safer, more efficient, and automated operations, and hence research into this field is the focus of many academic groups. Reactions where scalability in batch is problematic have often benefitted from being applied to continuous reactors, and there have been significant achievements in developing different approaches with many reactor designs being developed that address specific reaction difficulties.[6−8]

Photochemistry is an attractive synthetic tool, often deemed a green methodology, as it is frequently associated with efficient, mild and clean reaction conditions.[9] Recently the field has received much interest from both academic and industrial groups and has been reviewed comprehensively.[10−17] Continuous flow photochemistry presents significant advantages over more traditional batch reactions, as smaller path length reactors operating continuously can avoid issues such as light penetration, over irradiation and reactor fouling allowing for easier scale-up. For example photochemical reactions, where the penetration of light is of key importance, have benefitted greatly from a variety of innovative reactor designs.[17] In this paper we describe a new continuous flow reactor that we have applied to photochemical reactions involving oxygen. Various effective designs have been reported in the literature for these reactions; falling film,[18,19] bubble column,[20] spinning disc,[21−23] slug flow,[24,25] high pressure,[26−28] FEP tubular,[29] parallel tubular,[30] rotating thin film,[31] annular thin film,[32] milling,[33] and one recent design based on irradiating a nebulized liquid/gas mixture for singlet oxygen chemistry.[34]

Reactions with molecular oxygen (O_2) are highly desirable as they are highly atom economical and environmentally benign, and O_2 is readily available and abundant in the atmosphere, but scale-up can present issues. Molecular oxygen is often used as an oxidant or as a reagent, where it can be incorporated into molecules, in particular using photochemistry, where singlet oxygen ($^1O_2$) is generated and reacted with electron-rich functional groups.[15,35−42] Such reactions are not often carried out on a large scale because the use of pure oxygen poses several risks.[43] A recent example[34] that highlights the dilemma in scaling chemistry involving oxygen is a photoreactor design in which reaction solutions are nebulized into an atmosphere of O_2 or air creating fine droplets that are then irradiated. The large surface area of the droplets result in highly efficient reactions because the interface between gas and liquid is increased while the small diameter of the droplets means that light can more easily penetrate the solution. When flammable solvents are used, however, the problem of potential ignition or

Received: April 24, 2017
Published: July 3, 2017

DOI: 10.1021/acs.oprd.7b00153
Org. Process Res. Dev. 2017, 21, 1042−1050

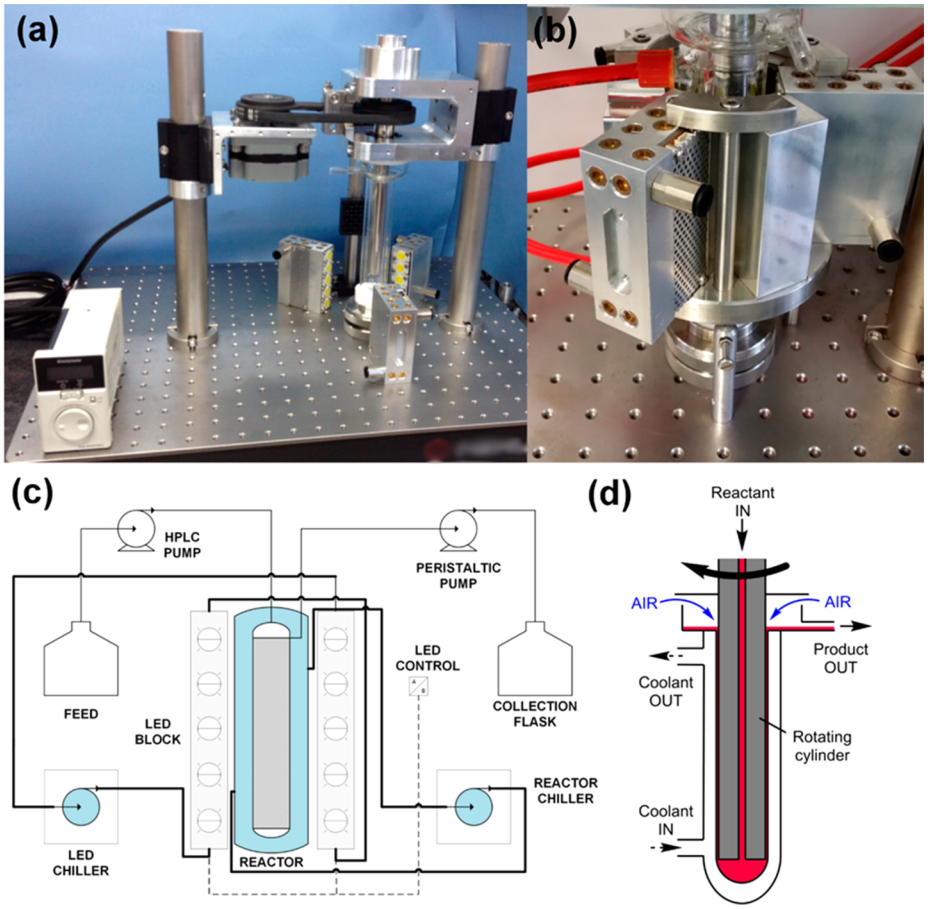

Figure 1. (a) Showing the deconstructed reactor with the motor and its control box. A drive belt connects the motor and the rotating cylinder. During operation a protective housing (not shown) contains the motor, belt, and moving parts. (b) Showing the LEDs and mirror blocks mounted place around the reactor. (c) Pipe diagram of the reactor setup showing the tubing connected to the reactor. Cooling is provided to the reactor by a recirculating chiller. The 3 LED blocks are connected in series and are cooled by a separate recirculating chiller. (d) A cross-section (not to scale) of the reactor showing the delivery and removal of reagents and the intake of air.

explosion of the solvent is always present. Safe operation is often realized by working below the limiting oxygen concentration (LOC), a region in which combustion is not possible.[44,45] In practice this is often achieved by using atmospheric or "synthetic" air (≤20% O_2 in N_2) instead of pure O_2. Unfortunately, using mixtures of gases often results in a loss of performance and slower reaction rates because lower partial pressures of oxygen result in lower concentrations of O_2 in the reaction mixture. Nonflammable solvents, such as supercritical CO_2 or H_2O, can be used to reduce the flammability issues associated with pure O_2; even though these solvents exhibit high gas solubility, many organic substrates are virtually insoluble in them.[46−48]

Continuous flow reactors can be beneficial when using pure oxygen,[49−51] as the precise delivery of reagents and gases can be controlled, thereby giving greater control over stoichiometry. Furthermore, the reactors can be small, and the chances of generating hazardous mixtures can be minimized. Continuous flow reactors can be pressurized and have high interfacial areas between the liquid and gas, allowing for greater dissolution of gases into the solution. Pressurized systems introduce additional hazards into the overall process. The ideal reactor would not be pressurized and would generate a large interfacial area for the reaction solution to interact with the oxygen, which would be supplied from the atmosphere. In essence, there is a trade-off between the inherent safety of the reactor and the volume of the gas phase and hence the area of the interface.

Here we describe a different approach with a large liquid volume and relatively small gas phase volume but with a high interface area because the gas is present as very small bubbles. Our design is based on so-called "vortex reactors"[52−59] which have been developed over the past 30 years. Here we bring together features from several previous reactors to make a surprisingly efficient reactor for photochemical reactions involving oxygen.[60]

A vortex reactor consists of a cylindrical outer vessel fitted with a smooth inner cylinder such that there only a relatively small gap between the inner and outer surfaces. The inner cylinder is rotated at a relatively high speed, e.g., 4000 rpm (revolutions per minute) and generates so-called "Taylor" or "Taylor-Couette" vortices, relatively narrow toroidal vortices threaded around the central cylinder; the precise nature of the vortices and hence the degree of mixing depends quite strongly on the dimensions of the reactor, the rotation speed of the rotor, and the properties of the fluid. There are published examples of vortex reactors operating in both vertical and horizontal orientation. Our design brings together three key features from earlier designs: (i) A vortex reactor for photochemistry, first demonstrated for the cleanup of polluted water using UV light and TiO_2 particles suspended in the water;[58] (ii) the use of a vortex reactor for the thermal

DOI: 10.1021/acs.oprd.7b00153
Org. Process Res. Dev. 2017, 21, 1042−1050

oxidation of benzaldehyde with O_2 or air (unlike our reactor this one operated horizontally).[52,56] (iii) A non-chemical report of an open-topped vortex reactor which drew air into the reactor from the room as the rotor was spinning.[57] Here we explain how we have incorporated these three features, together with modern high powered LED light sources, into a single reactor for photochemical oxidations and validated our design with dissolved oxygen studies. We then demonstrate its use with four different reactions. Among the advantages of our design is the fact that one does not require a separate supply of oxygen or air; the reactor draws whatever air is needed from the atmosphere of the laboratory.

RESULTS AND DISCUSSION

Reactor Design. The vortex reactor described in this study was built in a vertical orientation such that LED blocks could be more easily arranged around the outside of the reactor.[61] The reactor itself consists of a transparent Pyrex jacketed tube that is sealed at the bottom and contains a polished stainless steel cylinder with a narrow bore running coaxially through the center. The gap between the cylinder and the jacket is ca. 1 mm. The rotation of the stainless steel cylinder is provided by a spark free brushless motor that is housed to the side of the reactor and is connected to the cylinder using a drive belt. The top of the cylinder is held in place by an aluminum block to ensure that it remains truly vertical; the block also houses bearings to ensure that the rotor can be rotated freely at high speeds (Figure 1).

All moving parts, including the motor, drive belt, and the top of the cylinder with its bearings are housed inside an aluminum case so that they are contained during operation. The rotation speed is adjusted by a control box connected to the motor; the rotation speed can be set between 50−4000 rpm in both a clockwise and anticlockwise direction. To deliver the reagents into the reactor, the top of the reactor is fitted with a 1/16" stationary Swagelok fitting that attaches to 1/16" tubing that connects to a HPLC pump (JASCO Pu980). The reagents are delivered by this pump into the top of the reactor and down through the central bore of the stainless steel cylinder (Figure 1d). The jacketed Pyrex tube broadens out into a "cup" at the top to allow the reagent solution to exit the vortex zone of the reactor and be fed into an 1/8" PTFE tube connected to a peristaltic pump (Masterflex L/S). The flow rate of the peristaltic pump can be adjusted to suit the reagent delivery flow rate so that there is no build-up of solution in the top of the reactor. The presence of a free liquid surface at the top of the reactor allows air to be entrained in the low-pressure region generated by the rotation of the inner cylinder.

Around the reactor sits a circular mount that holds three LED blocks and three polished aluminum mirror blocks (Figure 1a−b). Each LED block consists of 5 × 1400 lm chips (Citizen Electronics part code: CL-L233-C13N1-C) and are positioned ca. 0.5 cm away from the jacketed reactor. The jacketed reactor and the LEDs are connected to recirculating chillers to ensure that the reactor temperature is constant by removing heat from operating the LEDs banks. The whole reactor is mounted on a base which is dampened to limit any vibrations created to by the reactor when it is operating at high rotation speeds. Two pillars provide a guide to ensure the housing containing the motor, drive belt, and the rotating cylinder are positioned correctly and at the same height. This allows for the whole set up to be easily removed, cleaned, and replaced. Further details of the reactor are provided in the SI.

The vortices within the annular gap occur when the dimensionless Taylor number that characterizes the flow conditions within the annulus is in excess of the critical value of 1700 (see SI for more details). To visualize the vortex flow structure, our reactor was modeled using computational fluid dynamics (CFD). Water was modeled inside an annulus of the same dimensions as the reactor with the inner cylinder rotating at 100 rad s^{-1} (ca. 955 rpm), giving a Taylor number of about 100,000, well above the critical value for the formation of Taylor vortices. Figure 2 shows the pattern of the vortices

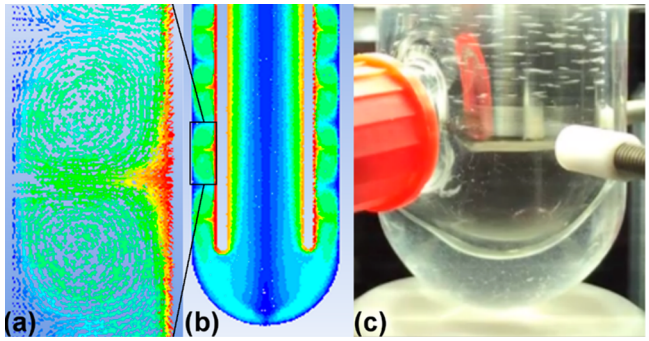

Figure 2. (a) Zoomed-in view of vortices generated by modeling the reactor with CFD, where the red areas, closest to the rotating shaft, show a higher velocity fluid, and the dark blue areas show a lower velocity fluid. (b) Generation of vortices along the length of the reactor using CFD; again the red areas, closest to the rotating shaft, show a higher velocity fluid, and the dark blue areas show lower velocity fluid. (c) Photograph showing the bubble streams as the reactor is spinning at 4000 rpm.

created inside the narrow gap of the reactor. The color shows the velocity of the fluid, red is highest and dark blue is lowest. Regular vortices can be observed along the length of the gap between the cylinders. In previous work, the boundaries between the vortices have been shown to contain gas and this is often visualized as bubbles or streams of bubbles within the reactor.[57] Further modeling and calculations regarding the generation of vortices in the reactor and description of our dissolved oxygen studies are provided in the SI. Figure 2c shows that, in reality, the streams of bubbles behave as predicted, at least at a qualitative level. Not only does CFD allow the fluid flow to be modeled, but it has the potential to be developed to model the chemical reaction with light. This will be done in further research, and such modeling can be used to develop scaled up and optimized reactors.

It has been shown previously that the UV−visible spectrum of an aqueous alkaline solution of pyrogallol can act as a quantitative measure of dissolved oxygen.[62,63] As oxygen is introduced, the initially colorless solution begins to turn yellow and then an increasingly darker brown color as more colored oligomeric and/or polymeric compounds are formed (Scheme 1). We used this approach to determine the effect of rotation speed on the rate of oxidation of the pyrogallol solution and, hence, as an indicator for the increased amount of O_2 at higher rotation speeds.

The results are shown in Figure 3. One can see from the spectra that, as the rotation speed increases, there is a corresponding growth in the intensity of the bands at 320 and 415 nm assigned to the products of oxidized pyrogallol. There is a linear increase in the growth of the bands between 0

DOI: 10.1021/acs.oprd.7b00153
Org. Process Res. Dev. 2017, 21, 1042−1050

Scheme 1. Oxidation of Pyrogallol with Air in an Alkaline Solution

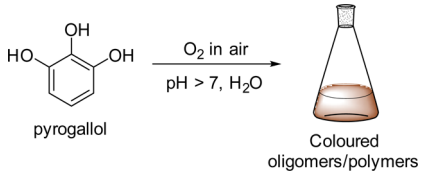

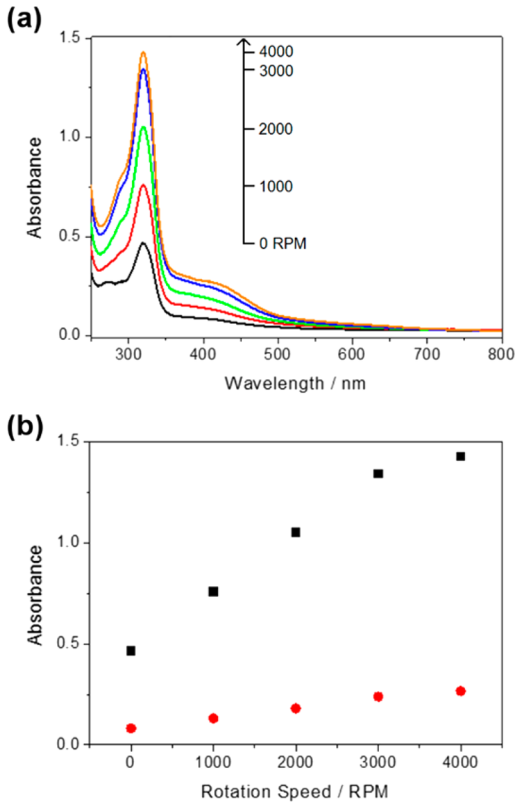

Figure 3. (a) UV–vis absorption spectra of aqueous basic pyrogallol solution (3 mM) measured after exiting the vortex reactor at several rotation speeds (0–4000 rpm); the flow rate was maintained at 1.0 mL min^{-1}. (b) Change in absorbance at 320 nm (■) and 415 nm (●) versus reactor rotation speed.

and 3000 rpm with minimal further growth observed at 4000 rpm, suggesting oxygen saturation of the solution.

These results are in agreement with the general conclusions of the modeling, which indicates that the flow regime in the reactor is well above the Taylor number for vortices to occur and that at higher speeds the mixing in the reactor will be more vigorous. As further confirmation, we employed the vortex reactor in several photochemical reactions involving oxygen; we predicted that the yield should scale with the rotation speed. Initially, the reactor was benchmarked against the some well-known reactions before being applied to a more challenging reaction involving both $^1O_2$ and $^3O_2$.

The initial benchmark of the reactor was the photo-oxidation of α-terpinene (**1**) (Scheme 2). The yield of ascaridole (**2**) was measured at different rotation speeds and flow rates.

A solution of **1** in ethanol using Rose Bengal (2 mol %) was flowed through the vortex reactor at a fixed flow rate of 0.5 mL min^{-1} with the LEDs at full brightness. Beginning with the cylinder stationary, the spinning speed was increased with samples taken at increments of 500 rpm. Two full reactor

Scheme 2. Photo-Oxidation of α-terpinene 1 to Ascaridole 2 and the Common Byproduct *p*-Cymene 3

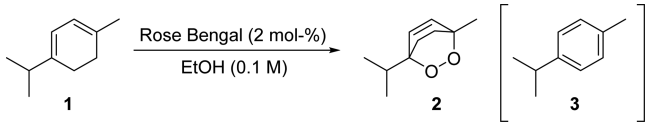

volumes were passed before the samples were taken to ensure that the reactor had reached a steady state. The conversion of **1** and the yields of **2** and **3** are plotted against rotation speed in Figure 4. Without any rotation, the yield of **2** was 35%; this improved as the rotation speed was increased up to 3000 rpm where the yield was 91%. Further increasing the spinning speed to 3500 and 4000 rpm had a detrimental effect on the yield of **2** due to the increased formation of *p*-cymene (**3**). It is apparent that as the speed was increased the reaction became more efficient. At the higher speeds the shear forces and mixing will be at their greatest; in addition gas–liquid interactions will be at their highest. In other words, the amount of oxygen available for reaction should increase as the rotation speed increases, and it would appear that O_2 is the limiting factor for the reaction at the slower spin speeds. To test this, reactions at 1000 and 1500 rpm were repeated with double the concentration of photosensitizer (4 mol %); the yields of **2** remained unchanged suggesting that the amount of oxygen is indeed the limiting factor at these speeds. In the case of 3500 and 4000 rpm, where the yield of **2** drops as more *p*-cymene (**3**) is formed as a byproduct, is possibly explained by the higher concentration of oxygen at these speeds. In this case it is likely that the photosensitizer is the limiting factor and the yield of **2** is less because of the competing oxidation reaction forming **3** with $^3O_2$. At 4000 rpm, when the concentration of Rose Bengal was doubled (to 4 mol %) the ratio of **2** to **3** improved from 3.5:1 (at 2 mol %) to 9:1 (at 4 mol %) suggesting that the amount of singlet oxygen generated was important for maintaining a high selectivity. When **1** was flowed in the dark as a control experiment, the amount of **3** increased with increasing rotation speed, where the *p*-cymene (**3**) yield was 4, 8, 11, and 15% at 1000, 2000, 3000, and 4000 rpm, respectively.

Next, the flow rate was changed while maintaining a fixed rotation speed because it is possible that an increase in upward flow could have an effect on the vortices. Flow rates of 0.5, 1.0, 1.5, and 2.0 mL min^{-1} were investigated (at 2000, 3000, and 4000 rpm). Increasing the flow rate, hence decreasing the residence time in the reactor, led to a decrease in the yield of **1** at all rotation speeds. At 1.5 mL min^{-1} and more so at 2 mL min^{-1}, the yields of **1** are very similar regardless of the rotation speed, suggesting that at these flow rates the amount of O_2 is comparable despite the difference in speed and suggests that the higher upward flow rates have a greater or overriding effect on the vortices (Figure 5).

To confirm that the faster rotation speeds, i.e., 4000 rpm, were the most efficient for reactions to be carried out, two more photochemical reactions involving singlet oxygen were run in the vortex reactor (Scheme 3). In the absence of a competing reaction with $^3O_2$ reaction, it was hypothesized that a rotation speed of 4000 rpm would be most efficient.

The photo-oxidation of furfural (**4**) with $^1O_2$ is an unusual reaction as the endoperoxide formed rearranges in the presence of a nucleophilic solvent (i.e., water or alcohol) and results in the breakage of a C–C bond to yield **5**. When this reaction was run in the vortex reactor, as expected, the yield increased with

DOI: 10.1021/acs.oprd.7b00153
Org. Process Res. Dev. 2017, 21, 1042–1050

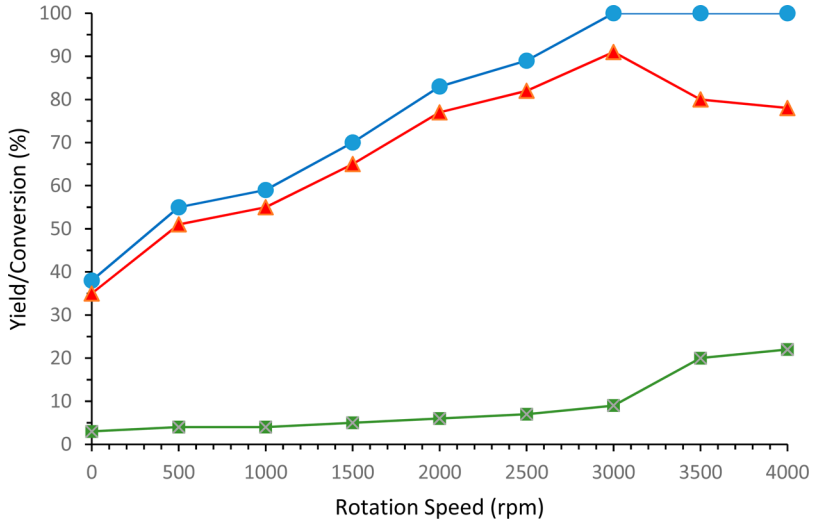

Figure 4. Showing the effect of rotation speed on the conversion of **1** (–●–) and the yields of **2** (–▲–) and *p*-cymene (–■–). The reaction was carried out on a 0.1 M solution of **1** in EtOH using Rose Bengal (2 mol %) with a fixed flow rate of 0.5 mL min^{-1} in air. The highest yield at 3000 rpm was 91% which is a productivity (prod.) of 2.73 mmol h^{-1} and a space time yield (STY) of 0.34 mmol h^{-1} mL^{-1}. [Productivity = conc. × flow rate × yield × 60 ; STY = productivity/reactor volume (8 mL)].

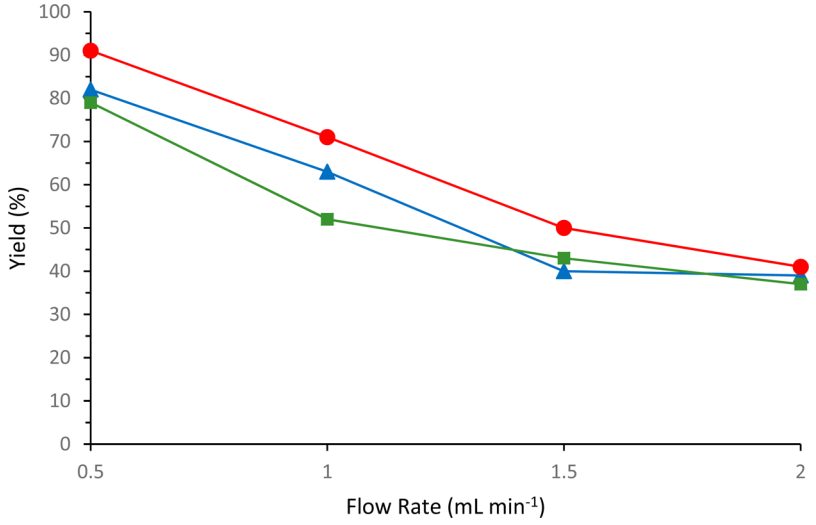

Figure 5. Showing the effect of flow rate on yield of **2** with a fixed spin speed. (–▲– = 2000 rpm, –●– = 3000 rpm, –■– = 4000 rpm) using a 0.1 M solution of **1** in EtOH with Rose Bengal (2 mol %). Under these conditions the speed at which the reaction mixture was pumped was adjusted and the yield of **2** monitored by ^{1}H NMR.

the rotation speed, and at 4000 rpm the yield was highest at 73% (Scheme 3a). The second reaction run was a photoredox reaction involving the generation of a superoxide radical anion ($O_2^{\bullet-}$) rather than the generation of singlet oxygen. The photocatalytic hydroxylation of phenyl boronic acid (**6**) proceeds from the incorporation of the superoxide radical anion and subsequent rearrangement to the phenol.[64,65] Using Rose Bengal as the photosensitizer and NEt(*i*-Pr)$_2$ (2 equiv) as the reductive quencher, the reaction was run at different spin speeds (Scheme 3b). At lower rotation speeds the conversion of **6** was incomplete and resulted in significant quantities of triphenylboroxine being formed; however, as the rotational speed was increased from 1000 to 4000 rpm and thereby the concentration of O_2, the formation of this trimeric byproduct was suppressed, and phenol (**7**) was formed as the major product. Despite the vortex reactor showing a lower throughput compared to the previously reported high pressure system (7.2 mmol h^{-1} vs 2.8 mmol h^{-1}), it does show a 19-fold increase in productivity when compared to that of previous batch reactions that have been carried out in air.[66] Furthermore, in previous high pressure reactions the addition of 67 molar equiv of air (or 13 molar equiv of O_2) at 2 MPa (20 bar) was required to obtain complete conversion of **6**.

In addition to photochemical reactions, a simple thermal oxidation reaction was run in the vortex reactor. Using Stahl aerobic oxidation conditions,[67,68] the oxidation of benzyl alcohol to benzaldehyde was carried out (Scheme 4). At room temperature the reaction gave little conversion, but increasing the temperature enhanced the conversion. As the reactor is jacketed, the reaction temperature can simply be controlled by adjusting the temperature settings on the recirculating bath. At 80 °C the product was obtained in a 85% yield directly from the reactor.

Our next example involves both photochemical and thermal steps and was carried out in the vortex reactor. Artemisinin combination therapy is one of the most preferred methods for

DOI: 10.1021/acs.oprd.7b00153
Org. Process Res. Dev. 2017, 21, 1042–1050

Scheme 3. Yields against Rotation Speed for the Photo-Oxidation for Furfural 4 and Phenyl Boronic Acid 6 in the Vortex Reactor[a]

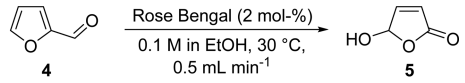

rpm	yield	prod. (mmol h^{-1})	STY (mmol h^{-1} mL^{-1})
1000	16%	0.48	0.06
2000	47%	1.41	0.18
3000	58%	1.74	0.22
4000	73%	2.19	0.27

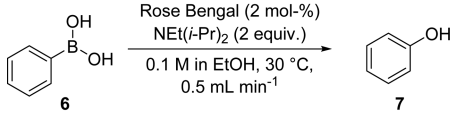

rpm	yield	prod. (mmol h^{-1})	STY (mmol h^{-1} mL^{-1})
1000	4%	0.12	0.02
2000	28%	0.84	0.11
3000	62%	1.86	0.23
4000	94%	2.82	0.35

[a]Prod. = productivity = flow rate × 60 × concentration × yield. [Productivity = conc. × flow rate × yield × 60; STY = productivity/reactor volume (8 mL)].

Scheme 4. Stahl Aerobic Oxidation Run in the Vortex Reactor Using Air[a]

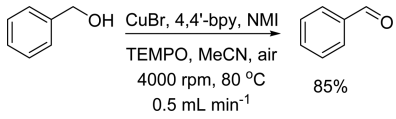

[a]Prod. = 2.55 mmol h^{-1}. STY = 0.32 mmol h^{-1} mL^{-1} [Productivity = conc. × flow rate × yield × 60 ; STY = productivity/reactor volume (8 mL)].

the treatment of malaria at present.[69,70] Hence there is increased motivation for more efficient and cost-effective routes to artemisinin (**8**) (Scheme 5),[71−73] especially now as the precursor dihydroartemisinic acid (**9**) can be prepared on scale using bioengineered yeast.[74] From **9** the synthesis of **8** proceeds in three steps (Scheme 5): (i) photo-oxidation of **9** with $^1O_2$, (ii) Hock cleavage and rearrangement of the hydroperoxide **10** facilitated by H^+, (iii) oxidation with triplet O_2 ($^3O_2$) and subsequent cyclization to afford **8**.

Scheme 5. Formation of Artemisinin (8) from DHAA (9)

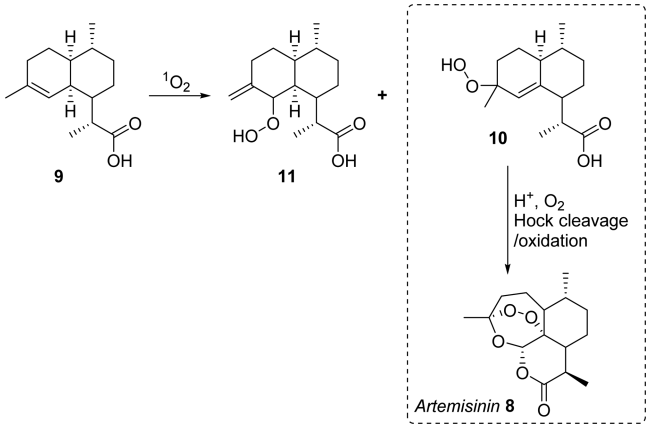

While there are three steps from **9** to **8**, the process is generally carried out as a one-pot procedure as acid can be added directly into the reaction mixture and the light source can be turned off to stop the generation of $^1O_2$.

The synthesis of artemisinin (**8**) has previously been reported by our group, with aqueous mixtures of THF or ethanol, which gave high yields for **8**, employed as green alternatives to more traditional reaction solvents, such as dichloromethane.[71] The previous batch protocol required irradiation for 1−5 h followed by up to 24 h stirring with bubbling O_2. With the high gas liquid interface in the vortex reactor, it was envisaged that the two steps could be carried out simultaneously and produce artemisinin (**8**) directly from the reactor. Initially, the steps were carried out independently to verify the photo-oxidation step in the vortex reactor. A 0.05 M solution of **9** in THF:H_2O (3:2) containing $[Ru(bpy)_3]Cl_2$ (0.1 mol %) was flowed through the vortex reactor at 0.5 mL min^{-1} at 4000 rpm and 30 °C. Complete conversion of **9** to peroxides **10** and **11** (9:1) was observed in the mixture obtained from the reactor outlet, so trifluoroacetic acid (TFA) was added to the collected mixture of peroxides which were then stirred with bubbling O_2 for 24 h to yield artemisinin in 60% as previously observed. When TFA was present in the reaction mixture from the beginning, the results obtained after the reactor were more complicated, and the overall conversion of **9** was reduced to 46% while the yield of **8** was obtained in just 5%. A variety of conditions were screened to increase the conversion of **9** and the yield of **8**, as summarized in Table 1.

Increasing the residence time by lowering the flow rate to 0.25 mL min^{-1} caused the yield of **8** increase accordingly to 10% (Table 1, entry 2), lower flow rates were attempted but led

Table 1. Optimization of the Yield of 8 in the Vortex Reactor[a]

entry	photosensitizer (mol %)[b]	solvent	TFA (equiv)	temp. (°C)	conv. (%)[c]	yield **8** (%)[c]
1	Ru (0.1)	THF:H_2O (3:2)	0.5	30	46	5
2[d]	Ru (0.1)	THF:H_2O (3:2)	0.5	30	64	10
3	Ru (0.1)	THF:H_2O (3:2)	0.5	10	100	0[e]
4	Ru (0.1)	THF:H_2O (3:2)	0.5	50	28	<1
5[f]	Ru (0.1)	THF:H_2O (3:2)	0.5	30	100	22
6	Ru (0.1)	toluene	0.5	30	31	20
7	DCA (0.5)	toluene	0.5	30	23	10
8	DCA (2.0)	toluene	0.5	30	41	22
9	TPP (0.5)	toluene	0.5	30	100	45
10	TPP (0.5)	toluene	0.5	25	100	50[g]
11	TPP (0.5)	toluene	0.5	20	100	39
12	TPP (0.5)	toluene	0.1	25	100	49
13	TPP (0.5)	toluene	1	25	100	48

[a]Reactions run with **9** (0.05 M in solvent), 4000 rpm, 0.5 mL min^{-1}. [b]Ru = $[Ru(bpy)_3]Cl_2$; DCA = 9,10-dicyanoanthracene; TPP = tetraphenylporphyrin. [c]Determined by ^1H NMR with biphenyl as an internal standard. [d]0.25 mL min^{-1}. [e]**10** 77%, **11** 23%. [f]The reaction mixture was recycled for 4 h. [g]Prod. = 0.75 mmol h^{-1}, STY = 0.094 mmol h^{-1} mL^{-1} [Productivity = conc. × flow rate × yield × 60 ; STY = productivity/reactor volume (8 mL)].

DOI: 10.1021/acs.oprd.7b00153
Org. Process Res. Dev. 2017, 21, 1042−1050

Scheme 6. Hock Cleavage Step from Peroxide 10 Leading to the Keto and Enol Intermediates, The Equilibrium of Which Likely Determines the Rate at Which the Second Oxidation Occurs[a]

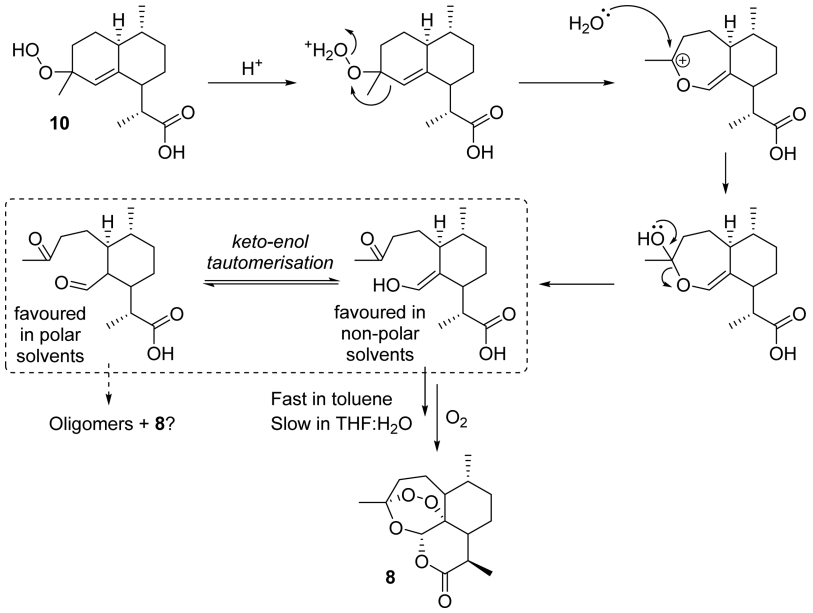

[a]In THF:H_2O the equilibrium lies further to the keto form; hence the formation of **8** is slow. In nonpolar solvents, the enol form is likely to be more favored which is demonstrated by an increase in the formation of **8**.

to irreproducible results. Lowering the temperature to 10 °C (Table 1, entry 3) slowed the Hock-cleavage step and yielded predominantly the peroxides **10** and **11**; however, this time, in a 3.4:1 ratio, while no **8** was observed. Increasing the temperature (Table 1, entry 4) proved detrimental to both the yield and conversion. When the material was recycled for a 4 h period, the yield of **8** peaked at 22%, but after 6 h the yield began to fall suggesting that product degradation was occurring under prolonged irradiation in the vortex reactor. Since the photo-oxidation step could be completed in one pass through the reactor, it is likely that sufficient oxygen was present; therefore, the limiting step was in the conversion of **10** to **8**. Considering the mechanism (Scheme 6) of the formation of **8** from **10** highlighted that the equilibrium constant of the keto and enol tautomers and hence the rate of formation of **8**. Typically, keto tautomers are usually more stable than the enol. This equilibrium, however, can be influenced by several different factors favoring either form; in this case the type of solvent appears to be the predominant factor.[75] In polar protic solvent mixtures where hydrogen bond donation to the ketones will be prevalent, the keto form will be favored, as demonstrated with aqueous THF or ethanol where the formation of **8** from **10** is slow, up to 24 h.[71] In less polar solvents, such as CH_2Cl_2, toluene, or perfluorinated solvents, the rate of formation of **8** from **10** is much faster; in this case, intramolecular hydrogen bonding between the enol and neighboring carbonyl will be predominant.[72,76]

When toluene was used as the reaction solvent, the yield of **8** increased to 20%, but $[Ru(bpy)_3]Cl_2$ had poor solubility; hence a poor conversion was observed (Table 1, entry 6). Switching the photosensitizer to 9,10-dicyanoanthracene (DCA) afforded a remarkably clean ^1H NMR spectra showing **8**, **9**, and little else, though both the yield and conversion were low (Table 1, entry 7). When the concentration of DCA was doubled, the conversion and yield increased 2-fold (Table 1, entry 8). When tetraphenylporphyrin (TPP) was used in the reaction, it initially reacted in the starting solution with TFA forming the protonated porphyrin ($TPP\text{-}H^+$), which is evident from the mint green color of the reaction mixture. When $TPP\text{-}H^+$ was used, full conversion was observed, and a 45% yield of artemisinin was obtained (Table 1, entry 9). When the temperature was reduced to 25 °C, the yield increased further to 50%. However, further reducing the temperature to 20 °C proved to be detrimental to the overall yield (Table 1, entries 10−11). Finally, the concentration of TFA was changed to 0.1 and to 1 equiv, however, both of these concentration yielded nearly identical results to using 0.5 equiv (Table 1, entries 12−13). The similarity in yield of **8** at the three concentrations of TFA is potentially indicative of greater mixing and mass transfer properties of the vortex reactor and requires further studying as the vortex reactor could be beneficial for other catalyst driven reactions.

CONCLUSION

A continuous flow vortex reactor has been developed that consists of a fast spinning rotor that sits tightly inside a jacketed vessel; as it rotates toroidal vortices are generated in the narrow space between the rotor and the jacket. This design brings together key features of other vortex reactors; having a light source for photochemistry and the introduction of air which is drawn in from the laboratory atmosphere as the reactor spins. CFD modeling of the parameters of the reactor gave visualization of the vortex stream inside the reactor; this is further supported by the visual appearance of streams of air bubbles as the reactor spins. Rotation speed appears to be directly linked to the amount of oxygen available to react, as at 4000 rpm, as reaction yields improved as the rotation speed was increased. The synthesis of artemisinin was carried out in the reaction, where the choice of solvent was key to successfully transferring the reaction from batch to continuous; in polar solvents, the final oxidation step was slow, but in nonpolar solvents it was fast enough that artemisinin could be obtained

DOI: 10.1021/acs.oprd.7b00153
Org. Process Res. Dev. 2017, 21, 1042−1050

directly from the reactor outlet in 50% yield when using TPP as a photosensitizer. The concentration of acid made little difference to the yield of artemisinin, suggesting that the intrinsic mixing properties of the reactor are well-tuned for catalytic reactions. It is possible that very low catalyst loadings could be applied to reaction without any substantial loss in efficiency. The reactors mixing properties could also be beneficial for biphasic or triphasic mixtures, where having a large interfacial area between two immiscible liquids or a liquid−gas mixture greatly improves efficiency. Simple modifications to the reactor would enable alternative gases to be applied; furthermore hazardous gases could be diluted with inert gases in the same way that oxygen is diluted in the air. There is potential for scale up of the vortex reactor as one could simply apply a rotor to an existing jacketed vessel much like the kind already used in process chemistry. We are currently developing a larger scale version of the vortex reactor and exploiting the current reactor in new chemistry. The CFD modeling will also be developed to include the photochemical reactions and effects of the second phase. This will give better understanding of the process to allow scale up with greater confidence.

■ ASSOCIATED CONTENT

Supporting Information

The Supporting Information is available free of charge on the ACS Publications website at DOI: 10.1021/acs.oprd.7b00153.

Further details of the reactor design, computational fluid dynamics (CFD), dissolved oxygen studies and experimental procedures, and representative ^{1}H NMR spectra (PDF)

■ AUTHOR INFORMATION

Corresponding Authors

*E-mail: mike.george@nottingham.ac.uk.
*E-mail: martyn.poliakoff@nottingham.ac.uk.

ORCID

Darren S. Lee: 0000-0002-8288-1838

Notes

The authors declare no competing financial interest.

■ ACKNOWLEDGMENTS

We thank EPSRC grants (EP/L021889/1), (EP/P013341/1), and the University of Nottingham EPSRC Impact Acceleration fund (EP/K503800/1) for supporting this work. The authors also thank the Bill and Melinda Gates Foundation (grant no. 1070294). We also thank M. Dellar, C. Dixon, P. Fields, M. Guyler, D. Lichfield, M. McAdam, and R. Wilson for technical support at the University of Nottingham. D.S.L. and C.A.C. would also like to thank Dr. Z. Abada, Dr. R. Horvath, E. N. DeLaney, and S. Miller for their useful discussions.

■ REFERENCES

(1) Britton, J.; Raston, C. L. *Chem. Soc. Rev.* **2017**, *46*, 1250−1271.
(2) Porta, R.; Benaglia, M.; Puglisi, A. *Org. Process Res. Dev.* **2016**, *20*, 2−25.
(3) Koenig, S. G.; Sneddon, H. F. *Green Chem.* **2017**, *19*, 1418−1419.
(4) Gavriilidis, A.; Constantinou, A.; Hellgardt, K.; Hii, K. K. M.; Hutchings, G. J.; Brett, G. L.; Kuhn, S.; Marsden, S. P. *React. Chem. Eng.* **2016**, *1*, 595−612.
(5) Plouffe, P.; Macchi, A.; Roberge, D. M. *Org. Process Res. Dev.* **2014**, *18*, 1286−1294.
(6) Gutmann, B.; Kappe, C. O. *Chim. Oggi.* **2015**, *33*, 18−24.
(7) Newman, S. G.; Jensen, K. F. *Green Chem.* **2013**, *15*, 1456−1472.
(8) Wiles, C.; Watts, P. *Green Chem.* **2012**, *14*, 38−54.
(9) Ciriminna, R.; Delisi, R.; Xu, Y. J.; Pagliaro, M. *Org. Process Res. Dev.* **2016**, *20*, 403−408.
(10) Skubi, K. L.; Blum, T. R.; Yoon, T. P. *Chem. Rev.* **2016**, *116*, 10035−10074.
(11) Romero, N. A.; Nicewicz, D. A. *Chem. Rev.* **2016**, *116*, 10075−10166.
(12) Remy, R.; Bochet, C. G. *Chem. Rev.* **2016**, *116*, 9816−9849.
(13) Ravelli, D.; Protti, S.; Fagnoni, M. *Chem. Rev.* **2016**, *116*, 9850−9913.
(14) Kärkäs, M. D.; Porco, J. A.; Stephenson, C. R. J. *Chem. Rev.* **2016**, *116*, 9683−9747.
(15) Ghogare, A. A.; Greer, A. *Chem. Rev.* **2016**, *116*, 9994−10034.
(16) Chen, M.; Zhong, M. J.; Johnson, J. A. *Chem. Rev.* **2016**, *116*, 10167−10211.
(17) Cambie, D.; Bottecchia, C.; Straathof, N. J. W.; Hessel, V.; Noel, T. *Chem. Rev.* **2016**, *116*, 10276−10341.
(18) Shvydkiv, O.; Limburg, C.; Nolan, K.; Oelgemöeller, M. *J. Flow Chem.* **2012**, *2*, 52−55.
(19) Jähnisch, K.; Dingerdissen, U. *Chem. Eng. Technol.* **2005**, *28*, 426−427.
(20) Yavorskyy, A.; Shvydkiv, O.; Limburg, C.; Nolan, K.; Delaure, Y. M. C.; Oelgemöeller, M. *Green Chem.* **2012**, *14*, 888−892.
(21) Van Gerven, T.; Mul, G.; Moulijn, J.; Stankiewicz, A. *Chem. Eng. Process.* **2007**, *46*, 781−789.
(22) Dionysiou, D. D.; Balasubramanian, G.; Suidan, M. T.; Khodadoust, A. P.; Baudin, I.; Laîné, J. M. *Water Res.* **2000**, *34*, 2927−2940.
(23) Barberis, K.; Howarth, C. R. *Ozone: Sci. Eng.* **1991**, *13*, 501−519.
(24) Levesque, F.; Seeberger, P. H. *Org. Lett.* **2011**, *13*, 5008−5011.
(25) Horie, T.; Sumino, M.; Tanaka, T.; Matsushita, Y.; Ichimura, T.; Yoshida, J.-i. *Org. Process Res. Dev.* **2010**, *14*, 405−410.
(26) Bourne, R. A.; Han, X.; Poliakoff, M.; George, M. W. *Angew. Chem., Int. Ed.* **2009**, *48*, 5322−5325.
(27) Han, X.; Bourne, R. A.; Poliakoff, M.; George, M. W. *Green Chem.* **2009**, *11*, 1787−1792.
(28) Hall, J. F. B.; Bourne, R. A.; Han, X.; Earley, J. H.; Poliakoff, M.; George, M. W. *Green Chem.* **2013**, *15*, 177−180.
(29) Hook, B. D. A.; Dohle, W.; Hirst, P. R.; Pickworth, M.; Berry, M. B.; Booker-Milburn, K. I. *J. Org. Chem.* **2005**, *70*, 7558−7564.
(30) Elliott, L. D.; Berry, M.; Harji, B.; Klauber, D.; Leonard, J.; Booker-Milburn, K. I. *Org. Process Res. Dev.* **2016**, *20*, 1806−1811.
(31) Clark, C. A.; Lee, D. S.; Pickering, S. J.; Poliakoff, M.; George, M. W. *Org. Process Res. Dev.* **2016**, *20*, 1792−1798.
(32) DeLaney, E. N.; Lee, D. S.; Elliott, L. D.; Jin, J.; Booker-Milburn, K. I.; Poliakoff, M.; George, M. W. *Green Chem.* **2017**, *19*, 1431−1438.
(33) Obst, M.; Konig, B. *Beilstein J. Org. Chem.* **2016**, *12*, 2358−2363.
(34) Ioannou, G. I.; Montagnon, T.; Kalaitzakis, D.; Pergantis, S. A.; Vassilikogiannakis, G. *ChemPhotoChem.* **2017**, *1*, 173−177.
(35) Ogilby, P. R. *Chem. Soc. Rev.* **2010**, *39*, 3181−3209.
(36) Margaros, L.; Montagnon, T.; Tofi, M.; Pavlakos, E.; Vassilikogiannakis, G. *Tetrahedron* **2006**, *62*, 5308−5317.
(37) Greer, A. *Tetrahedron* **2006**, *62*, 10613−10613.
(38) Clennan, E. L.; Pace, A. *Tetrahedron* **2005**, *61*, 6665−6691.
(39) DeRosa, M. C.; Crutchley, R. J. *Coord. Chem. Rev.* **2002**, *233*, 351−371.
(40) Frimer, A. A. *Chem. Rev.* **1979**, *79*, 359−387.
(41) Ohloff, G. *Pure Appl. Chem.* **1975**, *43*, 481−502.
(42) Kearns, D. R. *Chem. Rev.* **1971**, *71*, 395−427.
(43) Hone, C. A.; Roberge, D. M.; Kappe, C. O. *ChemSusChem* **2017**, *10*, 32−41.
(44) Osterberg, P. M.; Niemeier, J. K.; Welch, C. J.; Hawkins, J. M.; Martinelli, J. R.; Johnson, T. E.; Root, T. W.; Stahl, S. S. *Org. Process Res. Dev.* **2015**, *19*, 1537−1543.
(45) Brooks, M. R.; Crowl, D. A. *J. Loss Prev. Process Ind.* **2007**, *20*, 144−150.

DOI: 10.1021/acs.oprd.7b00153
Org. Process Res. Dev. 2017, 21, 1042−1050

(46) Bourne, R. A.; Han, X.; Poliakoff, M.; George, M. W. *Angew. Chem., Int. Ed.* **2009**, *48*, 5322−5325.
(47) Bourne, R. A.; Han, X.; Chapman, A. O.; Arrowsmith, N. J.; Kawanami, H.; Poliakoff, M.; George, M. W. *Chem. Commun.* **2008**, 4457−4459.
(48) Beckman, E. J. *J. Supercrit. Fluids* **2004**, *28*, 121−191.
(49) Mallia, C. J.; Baxendale, I. R. *Org. Process Res. Dev.* **2016**, *20*, 327−360.
(50) Hone, C. A.; Roberge, D. M.; Kappe, C. O. *ChemSusChem* **2017**, *10*, 32−41.
(51) Pieber, B.; Kappe, C. O. In *Organometallic Flow Chemistry*; Noël, T., Ed.; Springer International Publishing: 2015; Vol. *57*, p 97−136.
(52) Hubacz, R.; Wronski, S. *Exp. Therm. Fluid Sci.* **2004**, *28*, 457−466.
(53) Dutta, P. K.; Ray, A. K. *Chem. Eng. Sci.* **2004**, *59*, 5249−5259.
(54) Dluska, E.; Wronski, S.; Ryszczuk, T. *Exp. Therm. Fluid Sci.* **2004**, *28*, 467−472.
(55) Dluska, E.; Wronski, S. *Inz Chem. Procesowa* **2004**, *25*, 813−818.
(56) Dluska, E.; Wronski, S.; Hubacz, R. *Chem. Eng. Sci.* **2001**, *56*, 1131−1136.
(57) Atkhen, K.; Fontaine, J.; Wesfreid, J. E. *J. Fluid Mech.* **2000**, *422*, 55−68.
(58) Sczechowski, J. G.; Koval, C. A.; Noble, R. D. *Chem. Eng. Sci.* **1995**, *50*, 3163−3173.
(59) Kataoka, K.; Ohmura, N.; Kouzu, M.; Simamura, Y.; Okubo, M. *Chem. Eng. Sci.* **1995**, *50*, 1409−1416.
(60) Raston and co-workers have also described a photoreactor that involves rapid rotation, but it operates on quite a different principle because it generates a thin film with vortices on the inner surface of a rapidly rotating transparent tube. Gandy, M. N.; Raston, C. L.; Stubbs, K. A. *Chem. Commun.* **2015**, *51*, 11041−11044.
(61) In previous vortex photoreactors, the lamp(s) were placed in the center of the reactor rather than on the outside, thereby making the cooling of the lamp more complicated.
(62) Williams, D. D.; Blachly, C. H.; Miller, R. R. *Anal. Chem.* **1952**, *24*, 1819−1821.
(63) Duncan, I. A.; Harriman, A.; Porter, G. *Anal. Chem.* **1979**, *51*, 2206−2208.
(64) Pitre, S. P.; McTiernan, C. D.; Ismaili, H.; Scaiano, J. C. *J. Am. Chem. Soc.* **2013**, *135*, 13286−13289.
(65) Zou, Y. Q.; Chen, J. R.; Liu, X. P.; Lu, L. Q.; Davis, R. L.; Jorgensen, K. A.; Xiao, W. J. *Angew. Chem., Int. Ed.* **2012**, *51*, 784−788.
(66) Penders, I. G. T. M.; Amara, Z.; Horvath, R.; Rossen, K.; Poliakoff, M.; George, M. W. *RSC Adv.* **2015**, *5*, 6501−6504.
(67) Hoover, J. M.; Steves, J. E.; Stahl, S. S. *Nat. Protoc.* **2012**, *7*, 1161−1166.
(68) Hoover, J. M.; Stahl, S. S. *J. Am. Chem. Soc.* **2011**, *133*, 16901−16910.
(69) Paddon, C. J.; Keasling, J. D. *Nat. Rev. Microbiol.* **2014**, *12*, 355−367.
(70) Klayman, D. *Science* **1985**, *228*, 1049−1055.
(71) Amara, Z.; Bellamy, J. F. B.; Horvath, R.; Miller, S. J.; Beeby, A.; Burgard, A.; Rossen, K.; Poliakoff, M.; George, M. W. *Nat. Chem.* **2015**, *7*, 489−495.
(72) Kopetzki, D.; Levesque, F.; Seeberger, P. H. *Chem. - Eur. J.* **2013**, *19*, 5450−5456.
(73) Levesque, F.; Seeberger, P. H. *Angew. Chem., Int. Ed.* **2012**, *51*, 1706−1709.
(74) Paddon, C. J.; Westfall, P. J.; Pitera, D. J.; Benjamin, K.; Fisher, K.; McPhee, D.; Leavell, M. D.; Tai, A.; Main, A.; Eng, D.; Polichuk, D. R.; Teoh, K. H.; Reed, D. W.; Treynor, T.; Lenihan, J.; Fleck, M.; Bajad, S.; Dang, G.; Dengrove, D.; Diola, D.; Dorin, G.; Ellens, K. W.; Fickes, S.; Galazzo, J.; Gaucher, S. P.; Geistlinger, T.; Henry, R.; Hepp, M.; Horning, T.; Iqbal, T.; Jiang, H.; Kizer, L.; Lieu, B.; Melis, D.; Moss, N.; Regentin, R.; Secrest, S.; Tsuruta, H.; Vazquez, R.; Westblade, L. F.; Xu, L.; Yu, M.; Zhang, Y.; Zhao, L.; Lievense, J.; Covello, P. S.; Keasling, J. D.; Reiling, K. K.; Renninger, N. S.; Newman, J. D. *Nature* **2013**, *496*, 528−532.
(75) Reichardt, C.; Welton, T. *Solvents and Solvent Effects in Organic Chemistry*; Wiley-VCH, 2010.
(76) Turconi, J.; Griolet, F.; Guevel, R.; Oddon, G.; Villa, R.; Geatti, A.; Hvala, M.; Rossen, K.; Goller, R.; Burgard, A. *Org. Process Res. Dev.* **2014**, *18*, 417−422.

DOI: 10.1021/acs.oprd.7b00153
Org. Process Res. Dev. 2017, 21, 1042−1050